Macromolecular Research

Article

DOI 10.1007/s13233-018-6093-1

www.springer.com/13233 pISSN 1598-5032 eISSN 2092-7673

Simulation of Non-Isothermal Non-Newtonian Flow Behavior of PP for Various Injection Molding Screws and Comparison with Experimental Results

Seong-Yeol Park[†,1]
Min-Young Lyu[*,†,2]

[1] LG Chemical, LG Chemical Tech Center, Daejeon 34114, Korea
[2] Department of Mechanical System Design Engineering, Seoul National University of Science and Technology, Seoul 01811, Korea

Received December 12, 2017 / Revised February 12, 2018 / Accepted February 16, 2018

Abstract: Reducing injection molding cycle time is very important for improving productivity. In the cooling phase of injection molding, resin plasticization must be completed in the screw. This study examined the plasticization and flow behavior of polypropylene in injection molding screws using non-isothermal simulation. A standard screw and two types of barrier screws, the open-type, in which the barrier flight is open, and the closed-type, in which it is closed, were used. The geometry used in this simulation was wound using a channel model for a full three-dimensional flow simulation. Through non-isothermal simulation, the pressure distribution, melt flow, and temperature distribution were compared in terms of screw design. The experimental study revealed that in the open-type of the barrier screw, the solid bed and melt pool were well separated by the barrier flight, allowing for better melting than in the standard screw and the closed-type barrier screw. Simulation verified that resin melted better in the open-type barrier screw due to its easy inflow in the barrier flight and high temperature generation in the screw channel. The simulation results proved that the study of simulated flow and plasticization of resin in a screw is very useful for estimating screw performance.

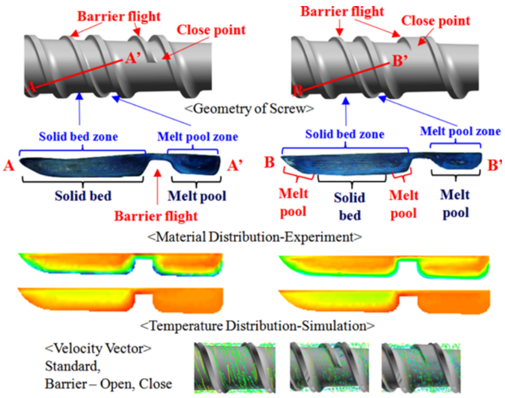

Keywords: injection molding screw, single screw, barrier screw, plasticization, non-isothermal flow simulation.

1. Introduction

The process of injection molding proceeds in the order of mold closing, injection, packing, cooling, mold opening, and ejecting. During the cooling phase, in the clamp unit, the part inside the mold is cooled, and in the injection unit, it is metered to determine the plasticization of the solid polymer.[1-3] Because the cooling phase takes up 70-90% of the entire injection molding process cycle time active research has been focused on developing cooling channel designs and optimal cooling times, to reduce the injection molding cycle time.[4,5]

In the injection molding process, the time allowed for plasticization of the resin in the screw is limited to the amount of time taken to cool the molded part for the next cycle. Therefore, when the cooling time is reduced, the time allowed for resin plasticization must also be equivalently reduced so that the next cycle can be executed without delay. As the demand for faster molding cycles increases, there is a pressing need for research on resin plasticization in injection molding screws.

Acknowledgment: This work was supported by the Industrial Fundamental Technology Development Program funded by the Ministry of Trade, Industry and Energy (MOTIE) of Korea (10051680, Development of high strength and environmental friendly polymer for 3D printing).

***Corresponding Author:** Min-Young Lyu (mylyu@seoultech.ac.kr)
[†]These authors equally contributed to this work.

Previous studies on the melting behaviors of polymers in a screw have mainly been focused on a single screw extruders. In 1959, Maddock conducted the first screw pull-out experiment, observed the cross-section of the resin, and published that there is a melt pool in the active flight, and a solid bed in the passive flight.[6] Tadmor presented a melting mechanism based on Maddock's experimental results in 1966,[7] and in 1967, published experimental results similar to Maddock's from a pull-out experiment on resin and processing conditions.[8] In 1967, Menges and Klenk reported that the melt pool is distributed across the passive flight and that the solid bed is distributed across the active flight.[9] In 1976, Dekker and Lindt observed that the solid bed is located at the center of the channel, that the melt pool is formed on the left and right of the channel, and that the thickness of the melt film gradually increases on the top and bottom of the channel.[10,11] Mount, III and Chung observed the melting behaviors of diverse polymers and tried to characterize the melting rate in terms of temperature and pressure in a screw.[12] In addition, Thompson and Wilczyński studied the melting mechanism with respect to the feed rate of the material.[13,14]

Melting mechanisms vary according to the screw geometry, resin shape, pressure profile, and molding conditions, but the mechanism examined by Maddock and Tadmor is dominant. A screw is divided into a feeding zone, melting zone, and metering zone, based on its function. In order to increase plasticization efficiency, the melting zone's length can be adjusted or its compression ratio changed.[15-17] Another method is to use a barrier screw, which increases melting efficiency by introducing a barrier flight to separate the solid bed and melt pool. In 1959, Maillefer was the first to apply for a patent on the barrier screw,[18] and development and research of barrier screw design has been carried out continuously since.[19,20] Studies on the melting and transportation of plastics in the screw of an injection molding machine and reciprocating extruder can be found in the literature.[21-24] Very recently, melting experiments involving injection molding screws were also performed by our group.[25,26]

Meanwhile, there has been analytical research on the resin flow inside the screw as well. Griffith studied the incompressible fluid inside the screw channel, and drew the conclusion that its flow and temperature distribution inside the channel were identical to those in an infinite channel.[27] Chung reviewed the theories for solid conveying, melting, and metering in a single screw and recommended melting theory.[28] Tadmor proposed the Flow Analysis Network (FAN) which utilizes the isothermal flow of a Newtonian fluid,[29] and Han and Lee studied the pressure distribution in the Maddock mixing head using the simulation method of the FAN.[30] Lyu and White researched the temperature, pressure, and fill factor for an environment in which the screw was set in rotational and reciprocating motions in a Buss Kneader.[31,32] Karwe and Jaluria studied the temperature distribution along the flow direction of the resin inside the screw assuming that the barrel had a constant temperature and the screw was insulated,[33] and Syrjälä conducted research on the three-dimensional flow and heat transfer in a linearly unfolded model of the material inside the screw channel.[34] Inoue *et al.* studied resin flow inside the screw using an isothermal, non-Newtonian fluid model, with Polyflow, a computational fluid dynamics (CFD) program.[35] Analytical and computational studies on the single screw of an injection molding machine can be found in the literature.[36-39] However, research that compares comprehensive experiments using various screw designs in an injection molding machine and non-isothermal flow simulation is very limited.

This study performed simulations of non-isothermal flows in single screws used for injection molding. The simulation results were then compared with the experimental results of previous studies.[25,26] Three types of screws were examined in this study: the standard screw, the open-type barrier screw, and the closed-type barrier screw. In the computer simulation, a non-isothermal, generalized Newtonian model was used to analyze the flow characteristics of the resin inside the screw. In previous studies, the melting of the resin inside the channel was observed using a screw pull-out experiment, and these results were used for comparison with the simulation results. Based on the simulation results, details of the flow and temperature of the resin inside the screw were observed, and the melting characteristics of the resin were examined in relation to screw design.

2. Screw Models and Material

The melting and flow behaviors in the melting and metering zones of screw extruder have been observed in many published articles, as described in the Section 1. Introduction. Melting length and material distributions in screw channels have

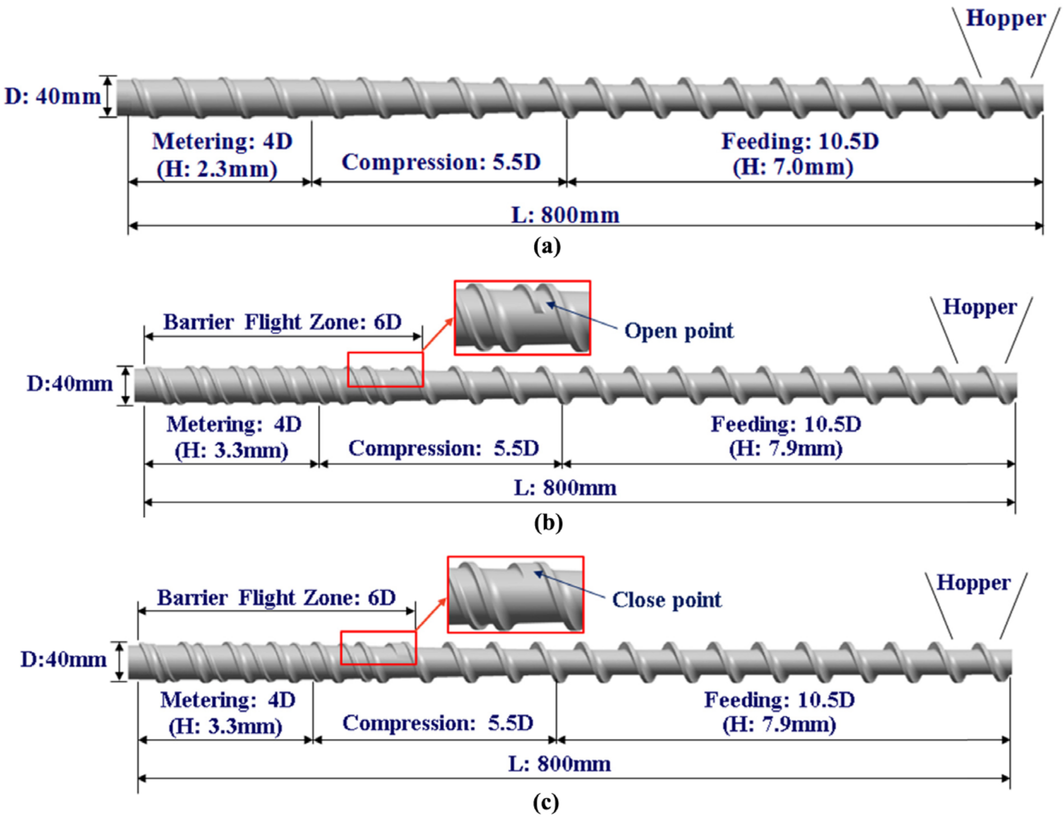

Figure 1. Geometry of the three screw designs. (a) Standard screw, (b) barrier screw: open-type, and (c) barrier screw: closed-type.

Table 1. Geometry data for the three screw designs

Screw	Standard screw	Barrier screw: open-type	Barrier screw: closed-type
Diameter (mm)	40	40	40
L/D	20	20	20
Depth in metering zone (mm)	2.3	3.3	3.3
Depth in feeding zone (mm)	7.0	7.9	7.9
Compression ratio	3.04	2.39	2.39
Shape of channel inlet in barrier flight	-	Open	Closed

been observed according to operating conditions and screw designs for single screw and screw configurations for twin screw extruders.

The screws that were studied here are the standard screw, open-type barrier screw, and closed-type barrier screw.

Figure 1 shows the three screw geometries, and Table 1 lists their relevant dimensions and characteristics. In the barrier screw for the extruder, the barrier flight starts at the first channel of the melting zone. In the injection molding machine, however, the screw moves backward as the resin melts, so in the two types of barrier screws in this study, the barrier flight starts at the fourth channel of the melting zone. Plasticization equipment for the screw pull-out experiment is described in the previous papers.[25,26]

The polypropylene (PP) homo-polymer (J150) from Lotte Chemical (S. Korea) was used as the material in this study. Its physical properties are listed in Table 2. The viscosity of PP is described in Section 4.

Table 2. Physical properties of polypropylene used in this study

Material property for PP (J150, Lotte Chemical)	
Density, ρ	0.9 (g/cm^3)
Specific heat, C_P	2100 (J/kg °C)
Thermal conductivity, k	0.15 (W/m °C)

3. Experimental observations

Experimental procedures performed in the previous study on the plasticization of PP in various screw designs and the results were summarized for comparison with the simulation results.

In order to facilitate the observation of the transfer and plasticization of resin, a 2% blue master batch was added to the natural resin. Figure 2 shows the location of the heater used to set the temperature of the barrel. The temperature settings for Heater 1 through Heater 6 were 230 °C, 220 °C, 220 °C, 220 °C, 200 °C, and 190 °C, respectively. The hopper section was set to 60 °C. The resin plasticization experiments using the three single screws proceeded as follows.[25,26]

First, the screw and RPM were selected and metered. Metering involves filling the hopper with resin, as the material proceeds forward as it melts along the screw channel due to the screw rotation. During metering, the pressure at the screw tip increases, which can force the screw to move backward, so the screw's back pressure was set to 30 MPs to prevent this. Then, metering was continued until a steady state was reached, where the back pressure, torque, and resin temperature became stable. In the steady state, the screw rotation was stopped, the band heater was turned off, the barrel was naturally cooled to room temperature, and then the screw was removed from the barrel. The resin inside the screw channel was separated, and its cross-section was observed.

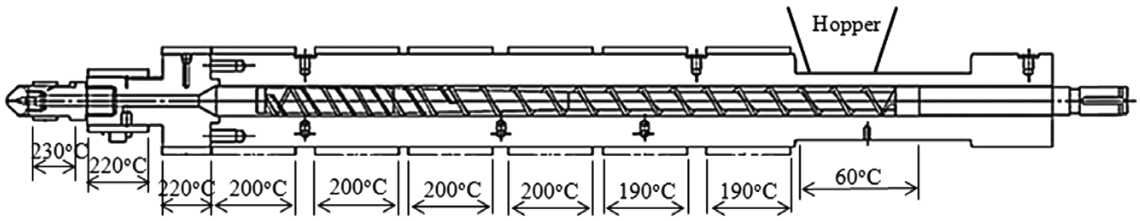

Figure 2. Temperature setting in the barrel.

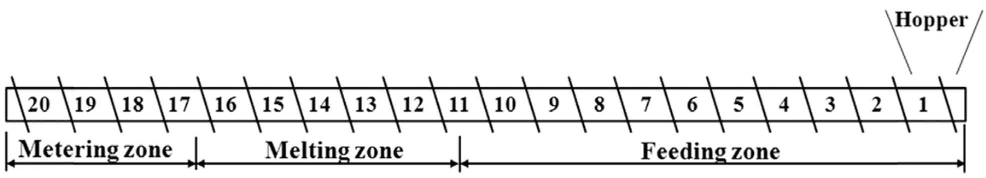

Figure 3. Channel number in a screw.

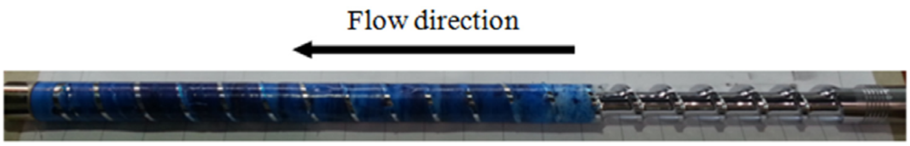

Figure 4. Material distribution in a screw.

Figure 3 shows the channel number in the screw. Channel 1 is where the resin is supplied to the Hopper, and there are up to 20 channels in the resin's transportation direction. Figure 4 shows the distribution of melted resin within the screw. Since a melt film is formed on the barrel surface, the channel that is the first to come into contact with the resin is the starting point of melting. The completion point of melting is the channel where the circulation flow of melt can be observed across the entire cross-section of the channel.

Figure 5 shows the cross-section of the resin in three types of screw channels at 70 RPM. Figure 5(a) shows the results for the standard screw. A melt film was observed on the surface in contact with the barrel in the 7th channel. The melt film forms due to the transfer of heat generated by friction between the resin and barrel surface and from the heater. In the 11th channel of the melting zone, where the channel's depth becomes lower, the separation of the melt pool and solid bed begins.

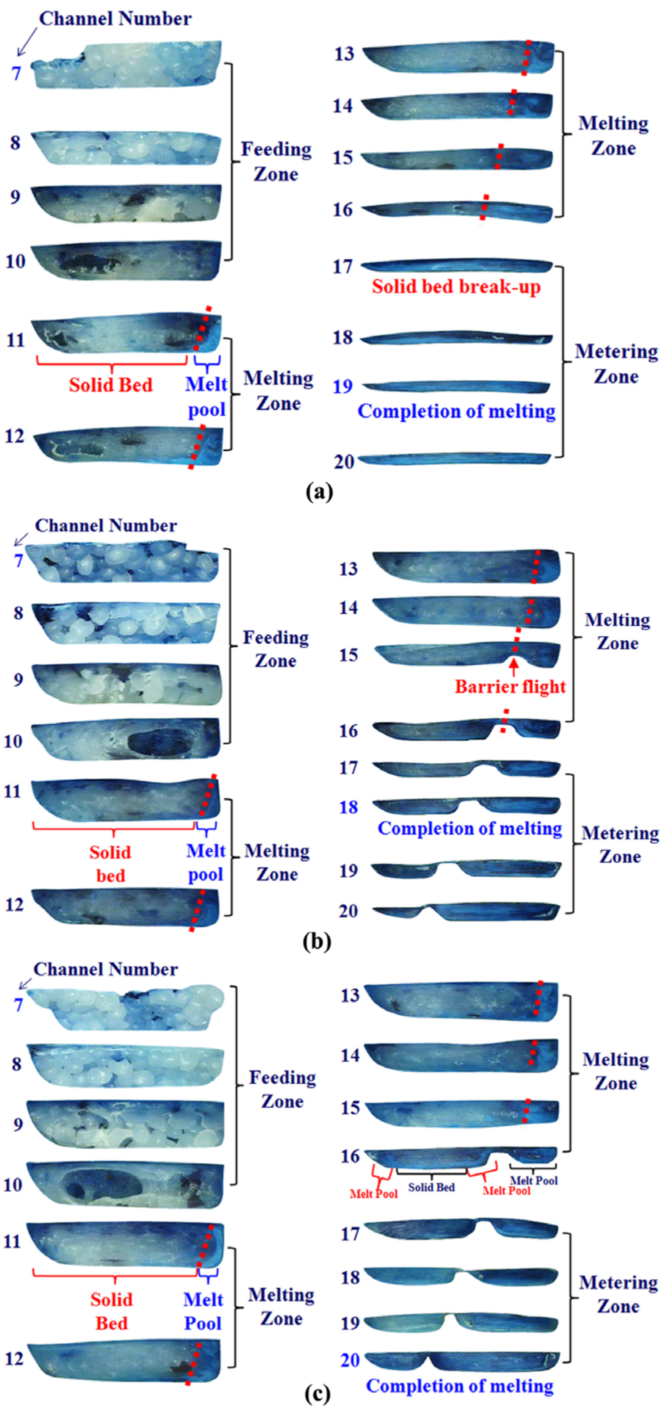

Figure 5. Materials in the screw channel of three different screws at 70 RPM. (a) Standard screw, (b) barrier screw: open-type, and (c) barrier screw: closed-type.

With the progression of flow, the melt pool increased, and the solid bed decreased. In the 17th channel, the solid bed was destroyed, and in the 19th channel, it was completely melted. This melting phenomenon showed a tendency similar to that of the melting mechanism studied by Maddock and Tadmor.[6-8] In the standard screw, the starting point of resin melting was the 7th channel, and its completion point was the 19th channel, making the melting length thirteen channels (7th to 19th channel). Figure 5(b) shows the experimental results for the open-type barrier screw. As in the standard screw, the melt film was formed in the 7th channel, and the solid bed and melt pool were found to be separated in the melting zone. The solid bed and melt pool were clearly separated by the barrier flight in the 15th channel, and the melting was completed in the 18th channel. Therefore, the melting length is twelve channels (7th to 18th channel), which is one channel shorter than for the standard screw. This barrier flight is thought to have increased the melting efficiency.

Figure 5(c) shows the results for the closed-type barrier screw. The melt film was formed in the 7th channel, and a complete melt pool was observed in the 20th channel. The melting length is fourteen channels (7th to 20th channel), which is two channels longer than for the open-type. In the melting zone with this barrier flight, the melt and solid resin were found to coexist in the solid bed zone up to the 17th channel. As seen in Figure 1(c), the melt pool channel is closed at the beginning of the barrier flight, so the resin flows into the solid bed region instead of the melt pool region. The barrier flight in this design is thought to be incapable of separating the solid bed and melt pool.

4. Computer simulation and results

4.1. Governing equation and constitutive equation

Material transportation in a single screw is classified into solid conveying, pressurizing and melting, and metering and pumping. The solid conveying zone has two phases of material since solid particles and air gaps co-exist between particles. The melting zone contains three phases, solid particles, air gaps, and molten material. The metering zone has one phase, molten material. It is difficult to simulate material transportation in a screw considering all three zones because the material has complex multi phases, and related theories and algorithms are not complete. Therefore, in the non-isothermal flow simulation one phase of molten material is considered in the screw channel and compared with the material transportation and temperature distribution depending on the screw design. Subsequently the melting behaviors of PP in a screw were characterized in terms of pressure, velocity, and temperature distributions.

The flow of the polymer melt inside the screw follows the equations of motion, and Eq. (1) is the equation of motion in a rectangular coordinate system.[31,32,40]

$$\frac{\partial(\rho u)}{\partial t}+\nabla\cdot(\rho u\vec{v})=\left(-\frac{\partial p}{\partial x}+\frac{\partial \tau_{xx}}{\partial x}+\frac{\partial \tau_{yx}}{\partial y}+\frac{\partial \tau_{zx}}{\partial z}\right)+\rho f_x \tag{1a}$$

$$\frac{\partial(\rho v)}{\partial t}+\nabla\cdot(\rho v\vec{v})=\left(-\frac{\partial p}{\partial y}+\frac{\partial \tau_{xy}}{\partial x}+\frac{\partial \tau_{yy}}{\partial y}+\frac{\partial \tau_{zy}}{\partial z}\right)+\rho f_y \tag{1b}$$

$$\frac{\partial(\rho w)}{\partial t}+\nabla\cdot(\rho w\vec{v})=\left(-\frac{\partial p}{\partial z}+\frac{\partial \tau_{xz}}{\partial x}+\frac{\partial \tau_{yz}}{\partial y}+\frac{\partial \tau_{zz}}{\partial z}\right)+\rho f_z \tag{1c}$$

where u, v, and w are respectively the velocities in the x, y, and z directions, and τ is the extra stress, whose relationship to the total stress σ is shown in Eq. (2):

$$\sigma = p\mathbf{I}+\tau \tag{2}$$

where p is the hydrostatic pressure and $\mathbf{I}$ is the unit tensor. The energy balance of the polymer melt in the screw is shown in Eq. (3). The derivation in this equation can be found in many references.[32,40]

$$\rho c\frac{DT}{Dt} = k\nabla^2 T+\sum \sigma_{ij}\frac{\partial v_i}{\partial x_j} \tag{3}$$

In this equation, k is thermal conductivity, i and j each takes the value of 1, 2, and 3, which represent the x, y, and z directions. Solving Eq. (1) and Eq. (3) simultaneously gives the flow characteristics and temperature distributions of melt in the screw channel.

The rheological model used in this study was the modified Cross law model, and the Arrehnius approximation was applied to express the change in viscosity with respect to temperature as in Eq. (4):

$$\eta = \frac{\eta_0}{(1+\lambda\dot{\gamma})^m}e^{-\alpha(T-T_0)} \tag{4}$$

where η_0 is the initial viscosity, λ and m are the Cross law model parameters, and $\dot{\gamma}$ is the shear rate. Figure 6 shows the measured shear viscosity curve for the resin and the result of curve fitting. The viscosity with respect to temperature was measured with a capillary rheometer (CEAST SR10). The results curve-fitted to the modified Cross law model which follows the Arrhenius approximation expressed by Eq. (4) are listed in Table 3.

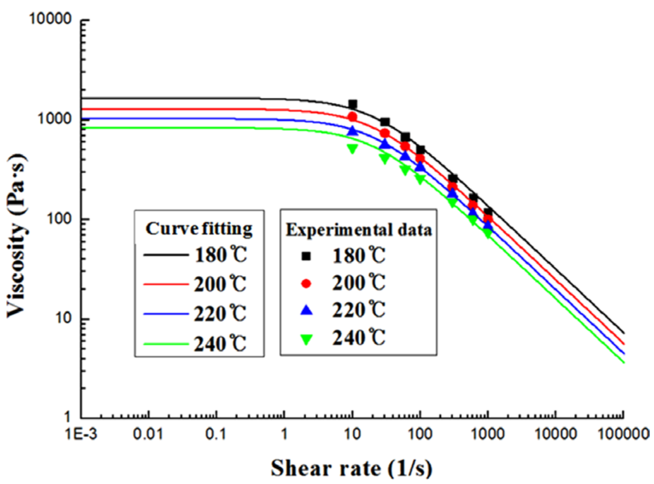

Figure 6. Experimental data and curve fitting results of viscosity used in study.

Table 3. Parameters in the modified Cross law model with Arrhenius approximation of the polypropylene melt used in this study

Zero shear rate viscosity, η_0	1278.28 (Pa·s)
Natural time, λ	0.0498
Cross law index, m	0.6391
First-order coefficient of the Taylor Expansion, α	0.0114
Reference temperature, T_0	200 (°C)

4.2. Method of simulation and boundary conditions

The finite element method (FEM) was used for the flow analysis inside the screw, and Polyflow, a commercial CFD program, was used. A non-isothermal, generalized Newtonian simulation was done on the resin flow inside the same three types of screws used in the experiment. The region of simulation was the melting zone (channels 11-16), in which the material shape was modeled. Since the melting zone geometry is different for all three screw types used in this study, the flow was analyzed with respect to screw design. Since the melting zone is where the resin actually melts, the melt and solid coexist, but for simplified simulation, it was assumed to be a melt when examining the flow and temperature distribution in terms of screw geometry.

Figure 7 shows the simulation model and boundary condition. The resin wound by the screw channel was modeled. Other studies on simulating the flow in a screw have adopted a flattened out model and were limited to two-dimensional geometry. However, in this three-dimensional flow simulation in a screw, a three-dimensional shape of the winding of the screw channel model was adopted. The inlet and outlet pressure values were set for the flow boundary condition. Since the pressure increases in the flow direction, the pressure was set to 0 MPa at the inlet and 7 MPa at the outlet, and ΔP was assumed to be 7 MPa, so that it increased in the flow direction of progress. During metering, the screw rotates, and the barrel is stationary.

As for the simulation condition, the relative motion of the barrel and screw was applied, so the inner surface of the barrel rotated in the direction opposite to that of the screw rotation, and the screw surface was stationary. The movement of the screw in the axial direction was ignored.

In the thermal boundary condition, the inlet temperature was set to 180 °C, and a convection was applied to the inner

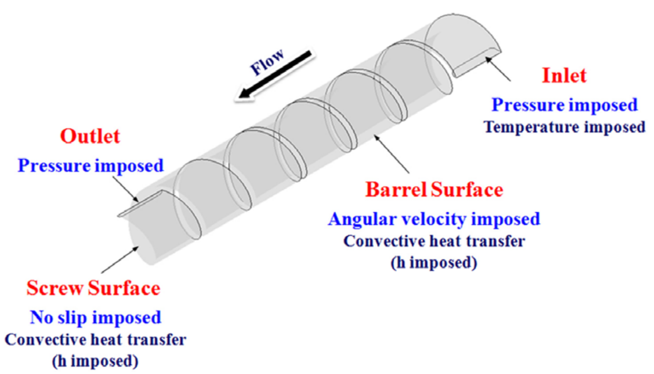

Figure 7. Flow and thermal boundary conditions.

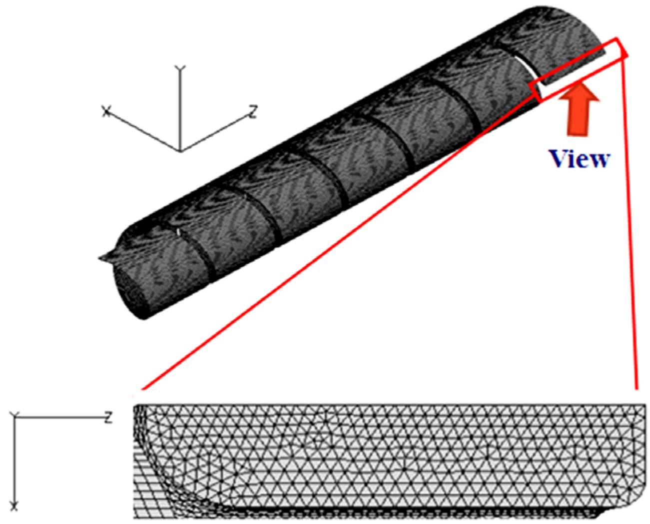

Figure 8. Three dimensional finite element mesh used for the simulation.

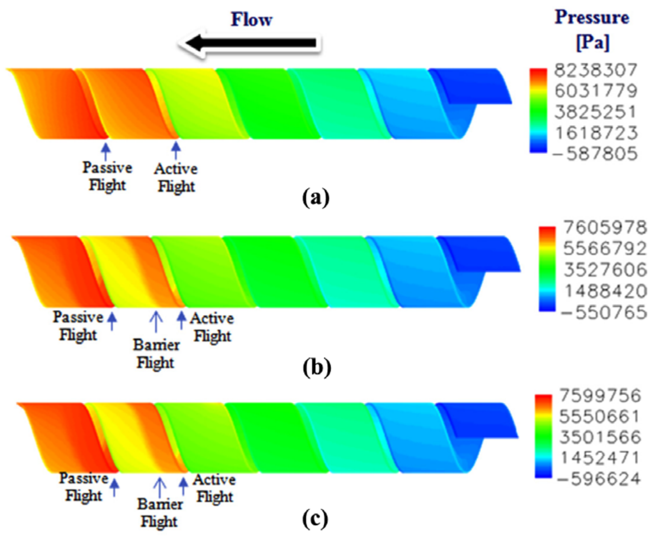

Figure 9. Pressure distributions in the three different screws. (a) Standard screw, (b) barrier screw: open-type, and (c) barrier screw: closed-type.

surface of the barrel and the surface of the screw. The convective heat transfer coefficient (h) between the barrel and resin was set to 2,000 W/m^2°C, and the barrel temperature was set to 200 °C, as in the experiment. The convective heat transfer coefficient between the screw and resin was set to 1,000 W/m^2°C, and the screw temperature was set to 90 °C.[31,32] Figure 8 shows the mesh for the simulation. It was formed by tetra and pyramid meshes, with about 800,000 elements.

4.3. Simulation results and discussion

Figure 9 shows the pressure distribution in the screw's melting zone. The pressure rise (ΔP) in the melting zone interval for the standard screw, open-type barrier screw, and closed-type barrier screw was found to be 8.83 MPa, 8.20 MPa, and 8.16 MPa, respectively. The pressure inside the screw channel increased in the direction of the melt flow along the channel. When the pressure rise (ΔP) in the screw increased, the amount of discharge decreased because of back flow pressure.[15,16,24]

The two types of barrier screws had a smaller pressure rise (ΔP) compared to the standard screw, which was found to be advantageous in the discharge of material. In a single channel, pressure decreased along the path from the active flight to the passive flight (in the cross channel direction), which was related to the circulation flow seen in the screw channel (Figure 10). In the two types of barrier screws, pressure in the melt pool channel was much higher than in the solid bed channel as shown in Figure 9(b) and (c).

Figure 10 shows the distribution of velocity in the cross channel direction in the standard screw's channel cross-section, as obtained from the computer simulation. Figure 10(a) shows the velocity vector, and Figure 10(b) shows the velocity profile in the measuring location shown in Figure 10(a). This phenomenon can be found in the calculations that took account of the flow in the cross channel direction.[15,16,24-26] Across the point 2/3 of the channel height, the velocity distributions were in opposite directions, which caused circulation flow. This circulation motion was related to the phenomenon in which pressure increased

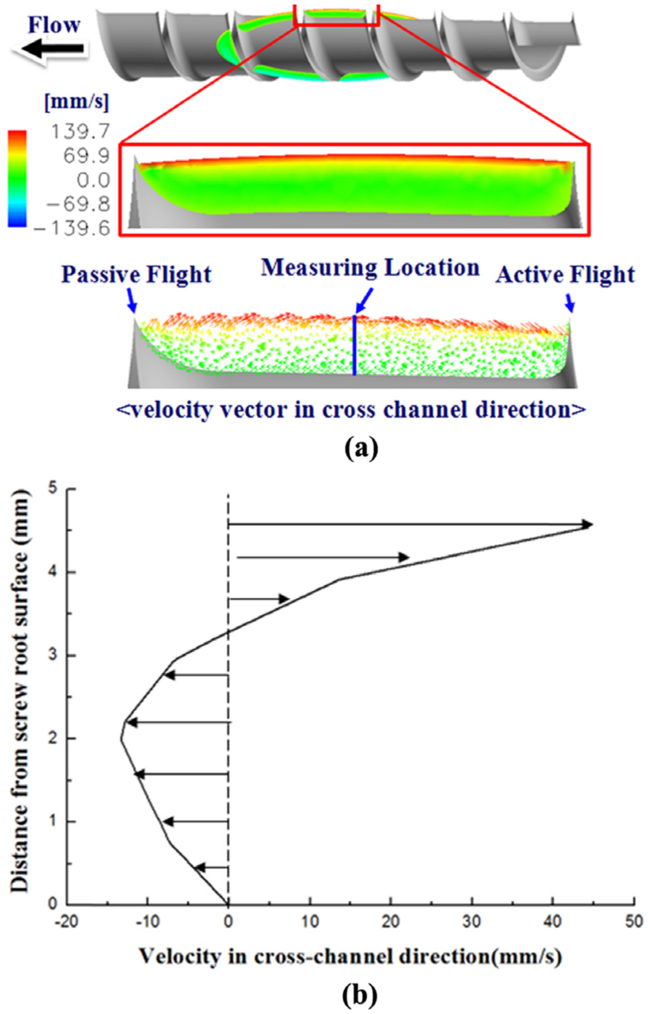

Figure 10. Velocity in the cross section of the screw channel. (a) Distribution of total velocity (x, y, z direction) in the screw channel, and (b) velocity profile in the cross channel direction.

in the path from the passive flight to the active flight (cross channel direction). The fundamental cause of this circulation motion

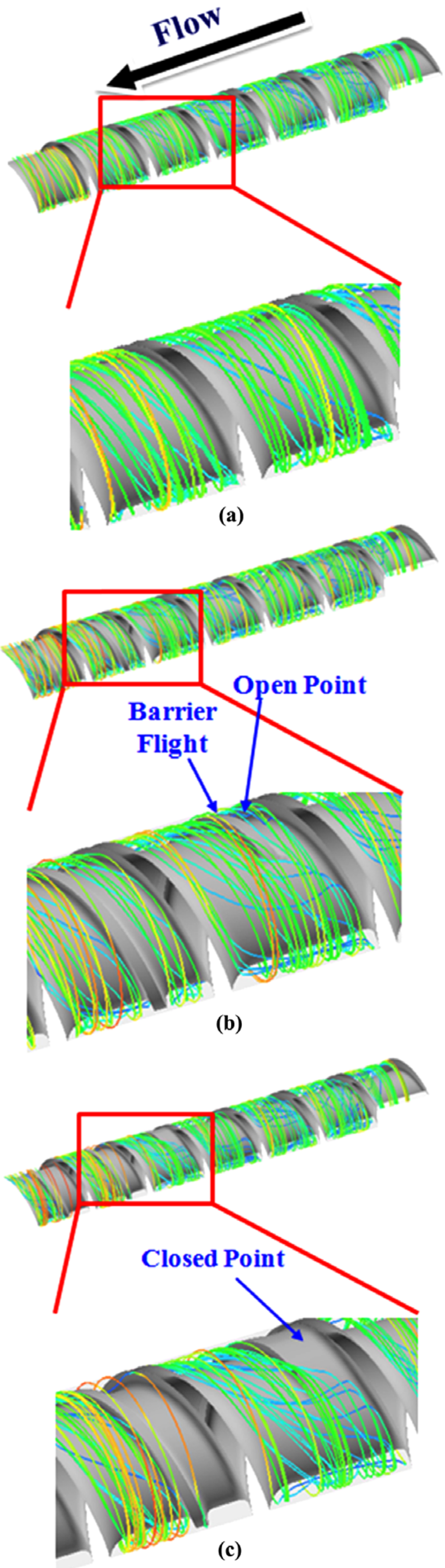

Figure 11. Streamline in the three different screws. (a) Standard screw, (b) barrier screw: open-type, and (c) barrier screw: closed-type.

Figure 11 shows the streamline of the resin flow in the three types of screws. The standard screw showed a uniform flow in the channel. As for the barrier screw, in the open-type, it could be seen that the material that flowed along the channel was divided into two branches of flow. It was thought that this flow would increase the melting efficiency by separating the solid bed and melt pool. In the closed-type barrier screw, the channel depth at the closed point was too shallow for the material to flow in, so all the material was transferred to the passive flight located on the left of the channel. That material flow was expected to have an adverse effect on melting, because it could not separate the solid bed and melt pool at the beginning of the barrier flight inside the channel.

The velocity vectors of flow in the two types of barrier screws are shown in detail in Figure 12. It can be clearly seen that the flow is separated by the barrier flight in the open-type screw as shown in Figure 12(b). However, the flow was not separated and all melt flowed to the channel of the passive flight side because was that the screw flight was at an angle to the direction of rotation. This was the reason that circulation flow in the experimental results was observed in the melt pool of the resin cross-section inside the screw channel.[24,25]

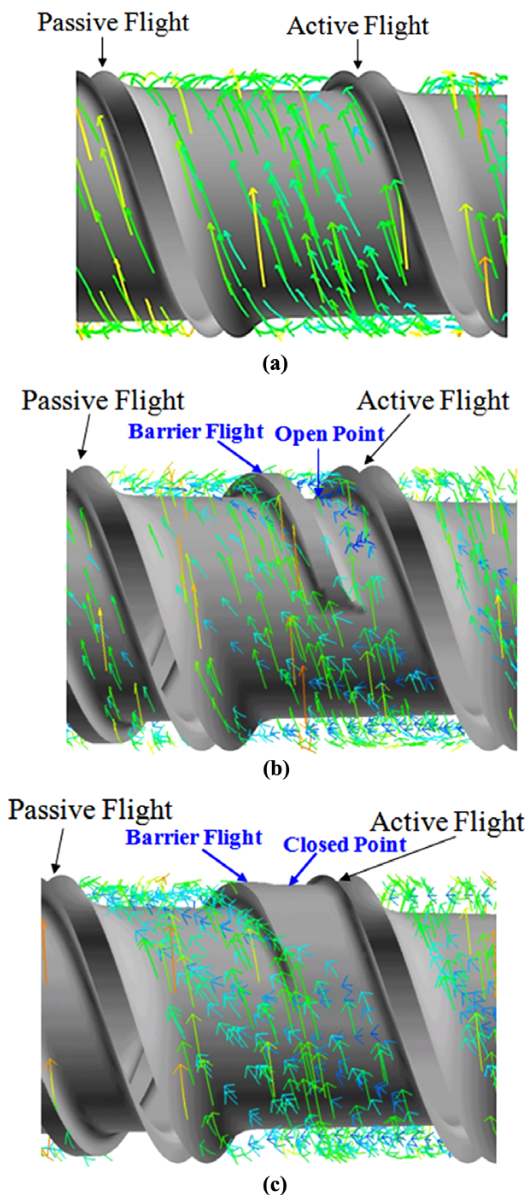

Figure 12. Velocity vector in the three different screws. (a) Standard screw, (b) barrier screw: open-type, and (c) barrier screw: closed-type.

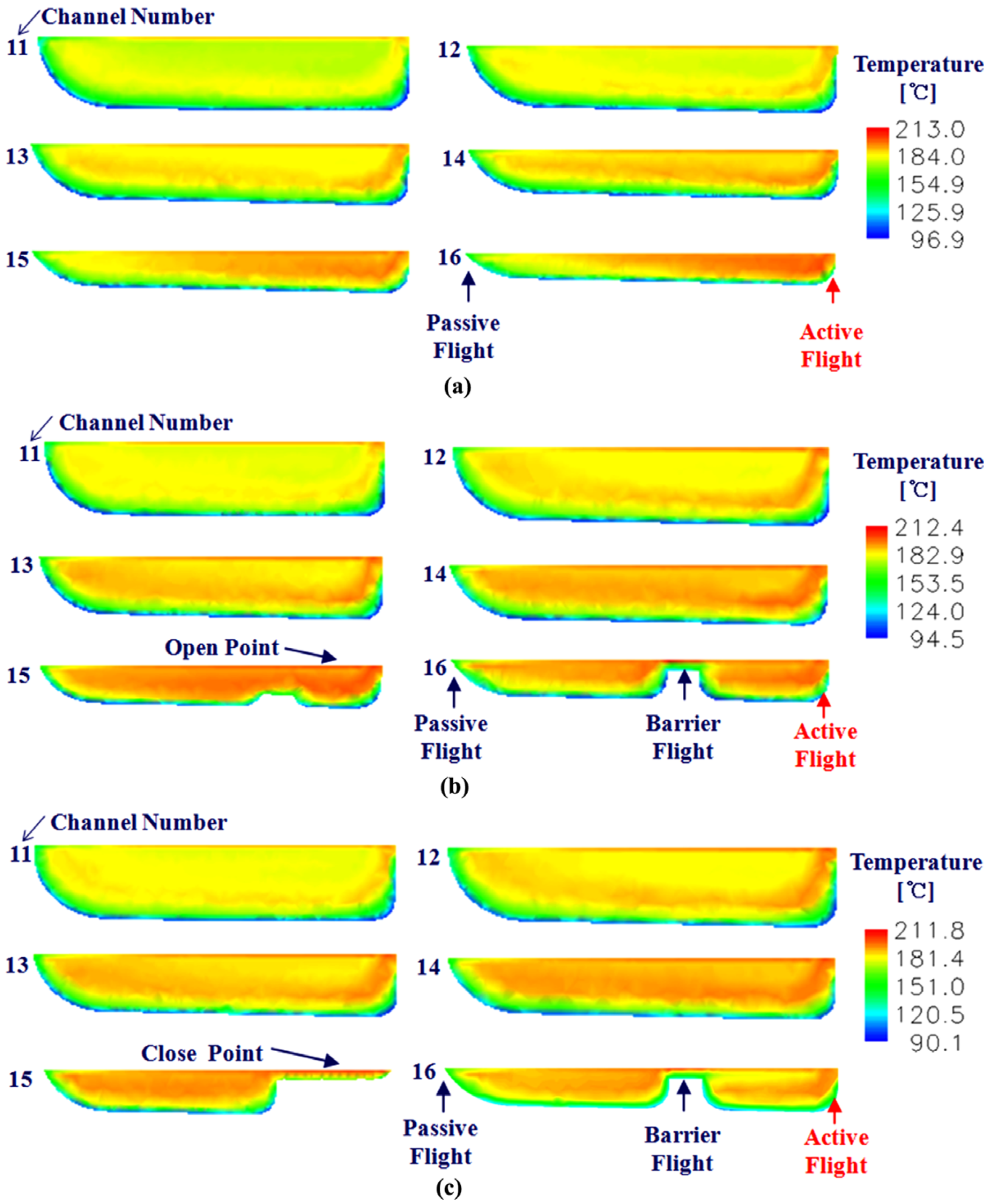

Figure 13. Temperature distributions in the three different screw channels. (a) Standard screw, (b) barrier screw: open-type, and (c) barrier screw: closed-type.

of the closed point at the beginning of barrier flight as shown in Figure 12(c).

Figure 13 shows the temperature distribution in the screw channel of the melting zone for the three screw types. Figure 13(a) shows that the temperature distribution was relatively uniform at the beginning of the channel for the standard screw, but along the channel, the temperature near the active flight increased. The reason was that the heat of the material which had a high temperature at the barrel surface was transferred as it flowed toward the active flight due to the circulation flow inside the channel as explained in Figure 10.

Comparing the open-type barrier screw (Figure 13(b)) and the closed-type barrier screw (Figure 13(c)), the 15th channel in the open-type had a higher and more uniform temperature distribution than that of the closed-type. The reason was thought to be that in the open-type, the flow of the material was smoothly

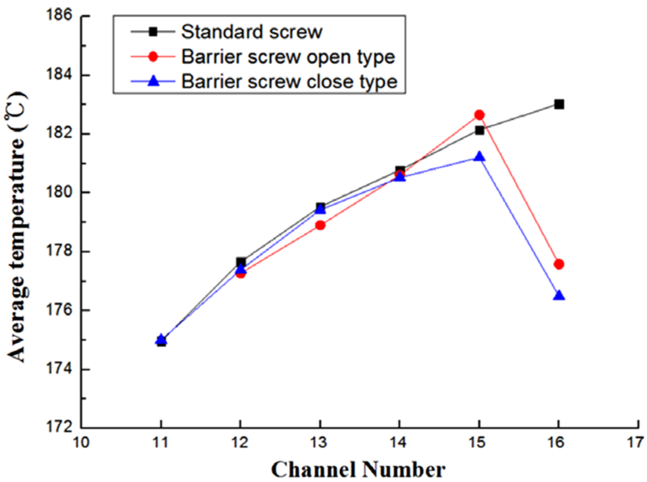

Figure 14. Average temperature in the three different screw channels.

separated by the barrier flight. Figure 14 shows the mean temperatures of the channels in the three screw types. A rise in temperature occurred as the material flowed along the channel. However, in the cases of the barrier screws, the temperature dropped rapidly at the 16th channel, because the screw's surface area was increased by the addition of the barrier flight. The open-type barrier flight had a higher temperature than the closed-type barrier flight from the 15th channel.

Except for from the boundary conditions set in Section 4.2, the simulation assumed there was no heat transfer on the screw surface, and for the heat transfer boundary condition the screw surface was assumed to be insulated. Other than the change from convection to insulation for the screw surface, the other boundary conditions were identical to the conditions set in the previous simulation (that is, theboundary conditions set in Section 4.2). Figure 15 shows the temperature distribution in the channel for the insulated condition.

As in the convection condition, low temperature was observed near the screw surface and the rise in temperature was apparent in the active flight side, due to the circulation flow in the standard screw. High temperature was observed near the screw surface in all the screws and became uniform as the flow proceeded.

For the insulation condition, there was no heat transfer on the screw surface, so there was a distribution of high temperature on the screw surface. As the flow proceeded the temperature in the channel increased and the temperature in the melt pool greatly increased and became uniform. Figure 16 shows the mean temperature of each channel. The temperature of the 16th channel was higher than in Figure 14, where convection heat transfer on the screw surface was accounted for. In the steady state during actual screw operation, the condition of the screw surface is thought to be in between convection heat transfer and insulation.

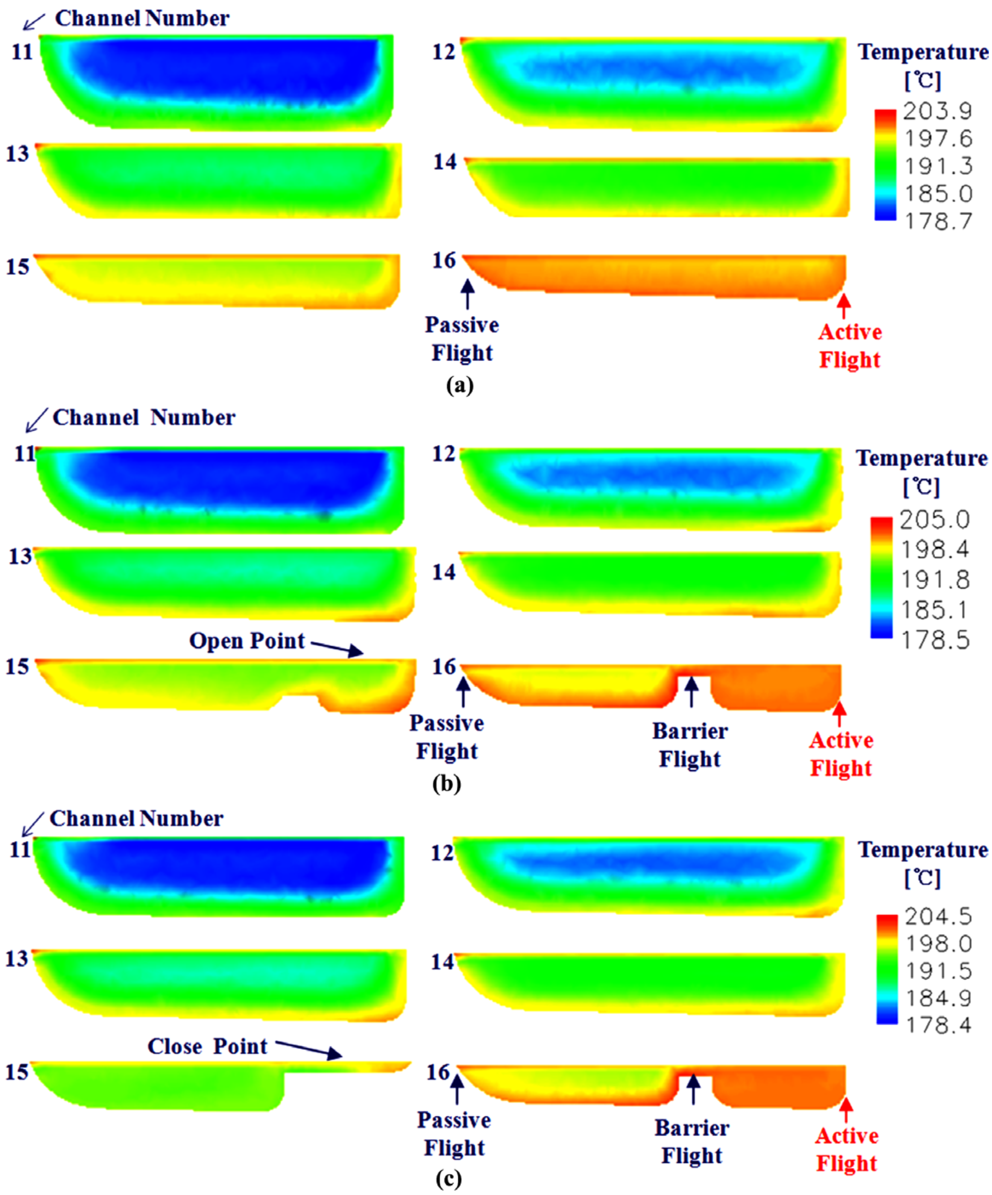

Figure 15. Temperature distributions in the three different screws for the thermal insulation condition at the screw surface. (a) Standard screw, (b) barrier screw: open-type, and (c) barrier screw: closed-type.

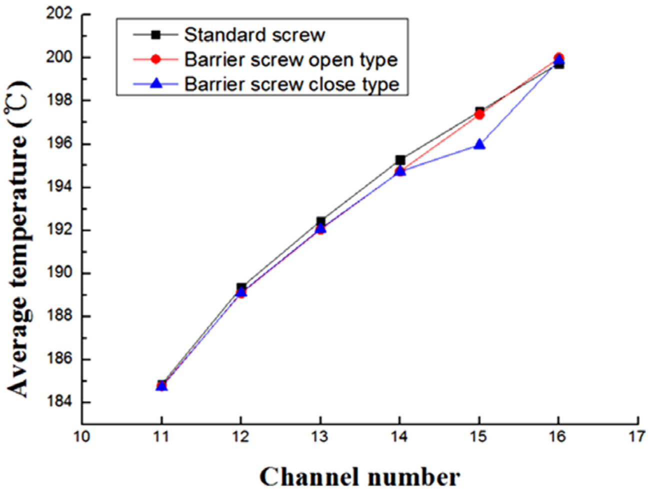

Figure 16. Average temperature in the three different screws for the thermal insulation condition at the screw surface.

5. Comparison of experiment and simulation

Figure 13(a) and Figure 15(a) are the temperature distribution simulation results in the channel at the melting zone for the conditions of convective heat transfer and insulation of the screw surface in the standard screw. And Figure 5(a) presents the experimental results of the melting zone for channels 11-16 in the standard screw. For the two thermal boundary conditions, convection and insulation, there was a rise in temperature near the active flight, and in the experimental results, the melt pool was observed near the active flight, and some melt was observed at the screw surface as well (11^{th} to 16^{th} channel in Figure 5(a)). The simulation results were considered valid, because melt was found where the temperature was high in the simulation.

Figure 9(a) presents the pressure distribution in the standard screw, which shows that the pressure at the active flight is high. It is believed that the solid bed was formed at the passive flight due to this pressure. In the experiment, the location of the the melt pool was found to be similar to the location where temperature was high in the simulation under the condition of insulation.

Figure 13(b) and Figure 15(b) are the temperature distribution simulation results at the melting zone inside the open-type barrier screw. The temperature was found to be higher near the active flight, and in the location of the melt pool in the presence of a barrier flight. Figure 5(b) presents the experimental results for channels 11-16 in the open-type barrier screw. Melt was observed at locations where the temperature was high in the simulation (11^{th} to 16^{th} in Figure 5(b)).

Figure 13(c) and Figure 15(c) are the simulated temperature distribution results at the melting zone inside the closed-type barrier screw, and Figure 5(c) shows the experimental results for channels 11-16 in the closed-type barrier screw. In the simulation, the temperature was found to be higher near the barrier flight and passive flight in the region of the solid bed in channel 16, and in the experiment, melt was observed in this location. The region in which the melt pool was observed in the experiment matched the region in which the temperature was found to be high in the simulation for the insulating condition.

6. Conclusions

This study examined the flow and temperature of PP in injection molding screws using simulation. The simulation involved a non-isothermal and non-Newtonian flow model with full three-dimensional flow geometry, wound by the screw channel model. The plasticization phenomena of PP reported for three screw designs, the standard screw, open-type barrier screw, and closed-type barrier screw, were then compared with the simulation results. It was found that the open-type barrier screw was more capable of effectively separating the solid bed and melt pool using the barrier flight, compared to the closed-type barrier screw, allowing for more effective melting. Ultimately, the melting of resin occurred best in the order of the open-type barrier screw, closed-type barrier screw, and standard screw.

In the computer simulation, the resin's pressure, temperature, streamline and velocity were observed in the melting zone of the three types of screws. Simulation results show that the pressure rise in the melting zone for the two barrier screws was smaller than that for the standard screw. The pressure inside the screw channel was found to be high at the active flight, and for this reason, the solid bed was located at the passive flight.

Observation of material flow showed that the barrier flight in the open-type barrier screw clearly separated the melt and solid, and had the greatest rise in temperature. Therefore, among the three screws used in this study, the open-type barrier screw was considered to be the most advantageous for resin plasticization.

This conclusion agreed with the experimental results as well. In the simulation, the boundary condition of insulation for the screw surface showed a greater rise in temperature at the active flight than in the boundary condition of convection heat transfer, which was the closest to the position of the melt pool observed in the experiment. The simulation results are considered useful for understanding resin melting and flowing phenomena in screws.

References

(1) T. A. Osswald, L. S. Turng, and P. J. Gramann, *Injection Molding Handbook*, Hanser Verlag, 2008.
(2) H. Y. Kim and M. Y. Lyu, *Polym. Sci. Technol.*, **20**, 157 (2009).
(3) L. Xie, B. Jiang and L. Shen, *Computational Fluid Dynamics Technologies and Applications,* InTech, 2011.
(4) M. Khan, S. K. Afaq, N. U. Khan, and S. Ahmad, *ISRN Mech. Eng.,* **2014**, (2014).
(5) M. Vishnuvarthanan, R. Panda, and S. Ilangovan, *Middle-East J. Sci. Res.*, **13**, 944 (2013).
(6) B. H. Maddock, *SPE Jl*, **15** 383 (1959).
(7) Z. Tadmor, *Polym. Eng. Sci.*, **6**, 185 (1966).
(8) Z. Tadmor, I. Duvdevani, and I. Klein, *Polym. Eng. Sci.*, **7**, 198 (1967).
(9) G. Menges and P. Klenk, *Kunststoffe*, **57**, 598 (1967).
(10) J. Dekker, *Kunststoffe*, **66**, 130 (1976).
(11) J. T. Lindt, *Polym. Eng. Sci.*, **16**, 284 (1976).
(12) E. M. Mount, III and C. I. Chung, *Polym. Eng. Sci.*, **18**, 711 (1978).
(13) M. R. Thompson, G. Donoian, and J. P. Christiano, *Polym. Eng. Sci.*, **40**,

2014 (2000).
(14) K. J. Wilczyński, A. Nastaj, A. Lewandowski, and K. Wilczyński, *Polym. Eng. Sci.*, **54**, 2362 (2014).
(15) C. Rauwendaal, *Polymer Extrusion*, Hanser Verlag, 2014.
(16) G. J. Morton-Jones, *Polymer Processing*, Springer, 1989.
(17) S. L. Rosen, *Fundamental Principles of Polymeric Materials*, Wiley, 1993.
(18) C. E. Maillefer, US Patent 3358327 (1967).
(19) M. Eshima, US Patent 5141326 (1992).
(20) A. L. Kelly, E. C. Brown, and P. D. Coates, *Polym. Eng. Sci.*, **46**, 1706 (2006).
(21) R. C. Donovan, *Polym. Eng. Sci.*, **14**, 101 (1974).
(22) C. Rauwendaal, *Int. Polym. Proc.*, **17**, 26 (1992).
(23) R. Steller and J. Iwko, *Int. Polym. Proc.*, **23**, 252 (2008).
(24) M.-Y. Lyu and J. L. White, *Int. Polym. Proc.*, **10**, 305 (1995).
(25) S.-Y. Park, G.-H Rhee, Y.-H. Nam, and M.-Y. Lyu, *Polym. Korea*, **40**, 414 (2016).
(26) S.-Y. Park, H.-S. Cho, G.-H. Rhee, Y.-H. Nam, and M.-Y. Lyu, *Polym. Korea*, **40**, 751 (2016).
(27) R. M. Griffith, *Industrial and Engineering Chemistry Fundamentals*, **1**, 180 (1962).
(28) C. I. Chung, *Polym. Eng. Sci.*, **11**, 93 (1971).
(29) Z. Tadmor, E. Broyer, and C. Gutfinger, *Polym. Eng. Sci.*, **14**, 660 (1974).
(30) C. D. Han, K. Y. Lee, and N. C. Wheeler, *Polym. Eng. Sci.*, **31**, 818 (1991).
(31) M. Y. Lyu and J. L. White, *Int. Polym. Proc.*, **12**, 104 (1997).
(32) M. Y. Lyu and J. L. White, *J. Reinf. Plast. Compos.*, **16**, 1445 (1997).
(33) M. V. Karwe and Y. Jaluria, *Numer. Heat Transfer*, **17**, 167 (1990).
(34) S. Syrjala, *Numer. Heat Transfer: Part A: Applications*, **35**, 25 (1999).
(35) A. Inoue, K. Morita, T. Tanaka, Y. Arao, and Y. Sawada, *J. Compos. Mater.*, **49**, 75 (2015).
(36) S. D. Lipshitz, R. Lavie, and Z. Tadmor, *Polym. Eng. Sci.*, **14**, 553 (1974).
(37) K. L. Yung, Y. Xu, and K. H. Lau, *J. Mater. Process. Technol.*, **139**, 170 (2003).
(38) K. L. Yung and Y. Xu, *J. Mater. Process. Technol.*, **117**, 21 (2001).
(39) C. Fernandes, A. J. Pontes, J. C. Viana, J. M. Nobrega, and A. Gaspar-Cunha, *Int. Polym. Proc.*, **29**, 1 (2014).
(40) R. B. Bird, R. C. Armstrong, and O. Hassager, *Dynamics of Polymeric Liquids: Vol. 1*, Wiley, 1987.